Experimental investigation of the wake of a lifting wing with cut-in sinusoidal trailing edges

S.L. Prigent[*], O.R.H. Buxton[†] and P.J.K. Bruce[‡]

Imperial College London, London SW7 2AZ, United Kingdom

The wake behind a NACA0012 wing at incidence with cut-in sinusoidal trailing edges (TE) is experimentally investigated. A wing model with interchangeable trailing edges is used to study their impact on the wake properties. Both vertical and span-wise traverses of hot-wires are done at different downstream positions, to obtain the downstream evolution of statistical properties and to perform spectral analysis. Stereoscopic particle image velocimetry is used to study the flow structure in a span-wise/cross-stream plane.

Span-wise inhomogeneity of the velocity deficit and of the wake width is observed and explained by the presence of a span-wise/cross-stream flow induced by the cut-in modifications. Spectral analysis shows a decrease of shedding intensity with shorter TE wavelength, with up to 57% reduction when compared to a straight blunt wing. Blunt sinusoidal TEs offer a reduction of span-wise correlation compared to a blunt straight one, which is mitigated when compared to an unmodified wing. A sharp cut-in design is also studied, that exhibits a more broad-band shedding spike at a lower frequency.

Nomenclature

c Chord

δ^* Boundary layer displacement thickness

Φ Cross power spectral density

γ^2 Two-point coherence

h Maximal bluntness at the troughs of the cut-in patterns

Re_c Chord-based Reynolds number

St Strouhal number based on h, $f.h/U_\infty$

---

[*]PhD student, dept. of aeronautics, Imperial College London
[†]Lecturer, dept. of aeronautics, Imperial College London
[‡]Senior lecturer, dept. of aeronautics, Imperial College London, AIAA member

American Institute of Aeronautics and Astronautics

St^* Strouhal number based on δ^*, $f.\delta^*/U_\infty$

St_K Stokes number

x Downstream position, originating at the tip of an unmodified TE

x^* Downstream position, corrected with the offset created by cutting into the TE

I.   Introduction

It is well known that modification of trailing edge geometry can have a significant influence on the performance of an airfoil. Previous studies[1,2,3,4] have shown that truncation of the aft part of the trailing edge could produce an increase of maximum lift coefficient. A structural benefit was also obtained, without the need to increase the maximum thickness of the airfoil, which is particularly interesting for large wind turbines. However, the introduction of trailing edge bluntness also led to an increase of drag, tempering any aerodynamic performance gain. Such blunt wings had a constant section, and further studies introduced a span-wise geometric variation to the blunt trailing edge[5,6,7] in an effort to increase the base pressure and therefore reduce base drag. Tanner[5] studied different blunt patterns and found that up to a 64% reduction in base drag, compared to a straight blunt trailing edge, could be obtained. Segmented trailing edges (castellation-like shapes) were found[6] to break down the vortex street structures generated by a straight blunt trailing edge by the introduction of stream-wise vorticity at the edges of the castellations. It was in fact understood that the span-wise vortices shed by the blunt trailing edge were responsible for low base pressure, which resulted in base drag increase.

These geometric modifications show the possible mitigation of the main flaw of blunt trailing edges. However, airfoil modifications should be considered in the context of key industrial challenges, such as open-rotors or wind farms, where self-noise or wake-blade interactions are particularly relevant. Vortex shedding at a straight blunt trailing edge not only impacts wing performance, but also wake properties as it generates a periodic vortex street over a large span-wise extent. It is therefore important to also understand how the shape modifications will affect the wake. Tombazis & Bearman[8] studied a non-lifting plate with a sinusoidal blunt trailing edge. The flow was found to be characterised by the co-existence of modes in the shedding in the wake, which inherently alter the single tone characteristic of blunt trailing edges.

In parallel, non-blunt shape modifications inspired by nature were investigated, with the aim of improving aerodynamic performance as well as reducing noise. Waviness was primarily studied at the leading-edge, with studies inspired by whales[9,10,11] , and showed the possibility to increase resistance to stall. It was introduced onto the trailing edge with studies such as Werle & Paterson[12] who focused on vertical undulation of the trailing edge. The authors observed that the modified geometry introduced a span-wise component to the

American Institute of Aeronautics and Astronautics

velocity, which seemed to re-energise the boundary layer and prevent stall. This translated into a 12% C_{Lmax} increase, with only a small corresponding increase in drag.

Howe[13] theoretically showed the ability of serrations to reduce noise production at the trailing edge in the case of flat thin plates. A numerical investigation was then conducted by Sandberg et al.[14] on serrations in flat extension plates for a lifting airfoil. Above a certain frequency threshold, the authors found that serrations would strongly decrease the trailing edge contribution to airfoil self-noise. An experimental investigation was also conducted on a full scale wind turbine with serrated extension plates,[15] and found up to a 3.2 dB reduction in noise.

A more recent approach has been to directly cut the serrations into the wing, to avoid the structural disadvantage of extension plates.[16] Chong et al. studied the acoustic impact of triangular cut-in serrations,[16] and found that for the turbulent boundary layer case, up to a 6.5 dB sound power reduction could be achieved, with better efficiency at high frequency than flat extension plates. However, the bluntness created at the root of the serration increases the low frequency noise due to vortex shedding. Nedić and Vassilicos[17] followed a similar approach, studying both triangular and multi-scale/fractal shapes cut into the trailing edge. Triangular serrations were found to improve the lift-to-drag ratio compared to an unmodified wing, with benefits depending on the serration angle. The best performance in terms of lift-to-drag ratio and vortex shedding intensity reduction was obtained for more complex fractal patterns,[17] with up to 8% increase in the former, compared to an unmodified wing.

These two studies have shown the possible benefits of using cut-in serrations on a trailing edge, in terms of aeroacoustic and aerodynamic performance, while offering a structural advantage. Nedić and Vassilicos[17] have given a first insight into the development of vortex shedding in the wake, with an interesting point being the dependence of shedding intensity on the angle of the serrations.

The effects of trailing edge shape modifications on the span-wise evolution of mean properties, and their downstream persistence, are crucial to better understanding how the wake is affected and to give a clearer picture of the flow structure. The span-wise distribution of vortex shedding and the identification of coherence also offer a deeper insight into the way vortex shedding develops in the wake. These aspects will be addressed in the current manuscript. The present study focuses on sinusoidal modifications, aiming to keep the shape as simple as possible to better understand the structure of the flow, and to avoid any angle discontinuity in the patterns. Based on the previous comments, a cut-in approach is chosen for the modifications.

American Institute of Aeronautics and Astronautics

II.   Experimental approach

A.   Wing model and trailing edge geometries

A NACA0012 wing with a removable TE sections is used, following Nedić and Vassilicos.[17] The wing itself has a chord $c = 150\,\text{mm}$, the boundary layer is tripped at $0.2c$ by a $5\,\text{mm}$ wide single strip of sand paper on both upper and lower surfaces, and the removable trailing edge section covers 92% of the $455\,\text{mm}$ span. The wing is placed at a $5°$ angle of attack which produces moderate lift with a large margin to stall which occurs for $\alpha_{stall} = 10 - 12°$.[17]

Experiments have been conducted in two low speed wind tunnels in the Department of Aeronautics at Imperial College London. The test section in both tunnels measures $457 \times 457\,\text{mm}$ and the background turbulence intensities were measured to be 0.15%. The tunnel speeds were set with a PID controller to match $Re_c = 150,000$ which compares to published data[17] and falls in the range of Reynolds numbers for both wings[18] and propellers[19] of small UAVs.

Because of the cut-in approach, the trailing edges exhibit bluntness in the troughs. The impact of bluntness is studied by introducing another type of geometry where the trailing edge is constrained to be sharp; this is allowed by modulating the aft part of the TE with a sinusoidal pattern instead of simply cutting into a standard NACA0012. An illustration of this approach and the parameters of the six trailing edges used in the present study are given in figure 1 and table 1.
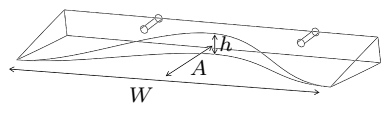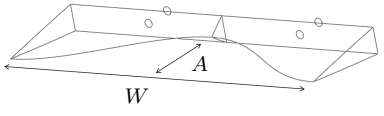
Name	Amplitude [mm]	Wavelength [mm]	Bluntness	Illustration
$S20W84B$	20	84	blunt	
$S20W40B$	20	40	blunt	
$S20W00B$	20	00	blunt	
$S20W84S$	20	84	sharp	
$S20W40S$	20	40	sharp	
$S00W00S$	00	00	sharp	
Nomenclature for S—W--†: **S**ine patterns, A=—[mm], **W**=--[mm],†**B**lunt or **S**harp				

Table 1: Trailing edges used in the study with geometric parameters.

B.   Hot-wire measurement apparatus

A custom probe holder was manufactured for each TE wavelength, to position three hot wires downstream of the peak, trough and mid-point (quarter wavelength from the trough), as illustrated in fig. 2a. Cross-stream traverses were then performed to cover the full vertical extent of the wake and study its downstream evolution.

American Institute of Aeronautics and Astronautics
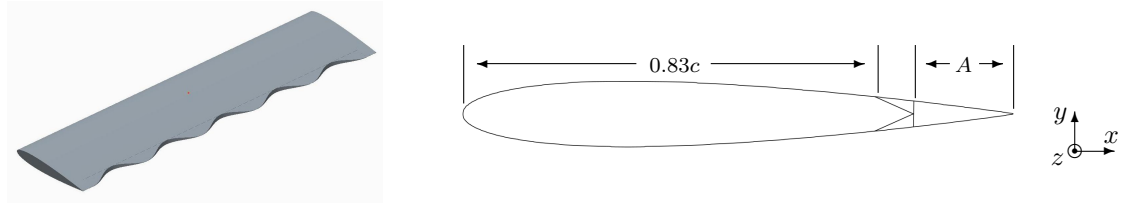
(a) 3-D model of the wing with blunt cut-in sinusoidal TE (to scale).

(b) Side sketch of blunt and sharp sinusoidal trailing edges (not to scale).

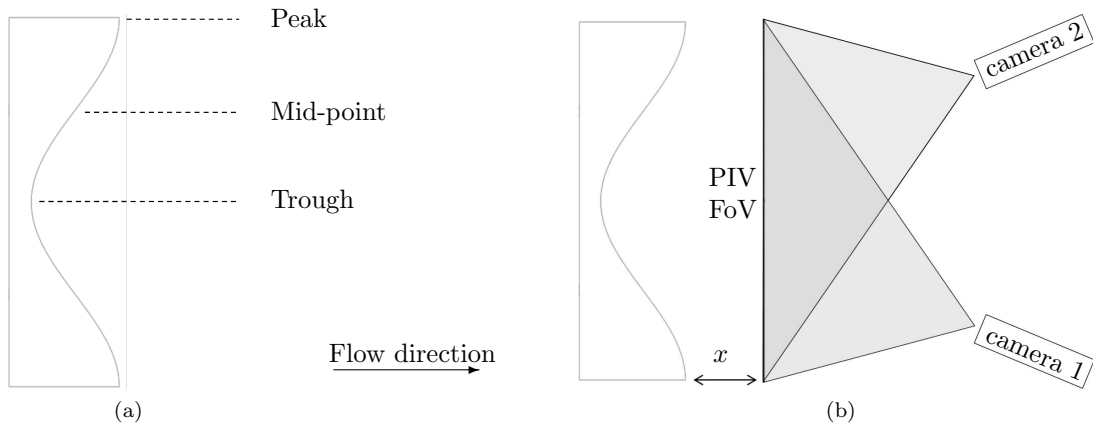Figure 1: Illustration of the trailing edges used in the study.

(a)

(b)

Figure 2: Hot wires located downstream of trough, peak and mid-point. Vertical traverses were conducted at different downstream positions (2a). Field of view of stereoscopic PIV apparatus, encompassing a full wavelength of $S20W84B$ (2b).

American Institute of Aeronautics and Astronautics

Three gold plated Dantec 55P01 hot-wires were used, connected to a Dantec StreamLine 90N10-Frame CTA powered by an isolated power supply. The square wave responses of the hot wires were all above 40 kHz, while a low-pass filter was set at 30 kHz. The sampling frequency of 100 kHz ensures that Shannon's principle is respected to avoid aliasing. Acquisition at each point lasted for 30 s to allow convergence of the statistics, covering about 16,000 shedding cycles. The over heat ratio was set at 1.8. Calibration was performed before each traverse, with a range of freestream velocities spanning from 8 m/s ($Re_c = 75,000$) to 23 m/s ($Re_c = 225,000$).

Span-wise traverses were also performed in the wake: one hot-wire being fixed at a trough, corresponding to the centreline, while a second is traversed away along the span-wise direction. The probes were mounted with the sensing wire orientated vertically to allow for smaller separation between them. The minimum separation for the different traverses is $1.5 - 2$ mm, and $\overline{U}$ and $\sqrt{\overline{u'^2}}$ were monitored when moving the probes together to ensure there was no aerodynamic probe interaction. Other technical details are as previously listed.

A gold plated Dantec 55P05 hot wire was used to investigate the boundary layer thickness at the trailing edge. A vertical traverse was performed with logarithmically spaced steps and a minimum step of $20\,\mu$m to ensure good accuracy. The acquisition frequency was the same as previously while the acquisition time at each position was set at 1 min. Traverses were performed for both the upper and lower surfaces.

C.   Stereoscopic PIV apparatus

Stereoscopic Particle Image Velocimetry (PIV) was conducted in a span-wise/cross-stream plane, $x/c = 0.04$ downstream of the trailing edge. Fig.2b illustrates the field of view (94×59 mm) which is normal to the stream-wise direction and encompasses a full wavelength of $S20W84B$.

The illumination was made using a Litron LDY300 (Nd:YLF) laser, and two Phantom M310 cameras (25.6×16.0 mm/1280×800 px sensors) with Nikon $135\,mm\ f/2\ DC$ lenses were used for imaging. The illumination and imaging set-up was controlled by the commercial software LaVision's Davis. Data was acquired at 250 Hz with a double frame separation time of $12\,\mu$s.

The tunnel was seeded with a water/glycol (4:1) solution with the particles' diameter being $d = 2 - 3\,\mu$m. Stokes number, defined as

$$St_K = \frac{t_0 U_b}{l}; \text{ where } t_0 = \frac{\rho d^2}{18\mu}, \tag{1}$$

with U_b the local mean velocity and l the PIV spatial resolution, gives a value of $St_K = 0.08$, within the $St_K << 1$ range, which is the criteria for particles to behave as tracers.

Images were pre-processed to subtract the background luminosity, and a sliding background average was

American Institute of Aeronautics and Astronautics

applied to account for non-uniformity in the illumination. Recursive processing was done with an initial window size of 64×64 px, final window size of 32×32 px and 75% overlap, giving a spatial resolution of 1.8 mm. The velocity vector fields were then post-processed to remove spurious vectors, with rejected vectors being fewer than 1%.

III.   Results

A.   Mean properties

The mean velocity profiles, obtained from hot-wire anemometry measurements behind the trough, peak and mid-point, are plotted in fig. 3a for wing $S20W84B$ at $x/c = 0.04$. The three profiles collapse on the whole traverse except at the center of the wake, where the maximum velocity deficit exhibits a span-wise dependence. One also notices that the mean velocity collapses to the free stream under the wing, within a margin of 0.5%, while an increase of up to 7% is observed above the wing (out of plot range in fig. 3a). There is expected to be an increase of the speed above the wing, as it is a lifting body, and this effect is further increased by the proximity of the upper wall of the wind tunnel (only $1.5c$). Fig. 3b shows the turbulence intensity profiles of the three span-wise locations. The trough's profile shows a higher turbulence intensity as well as a wider shear layer.

It is logical to expect higher turbulence intensity in the wake of the trough, because it is blunt, however it would also be expected to have a higher velocity deficit, contrary to what is observed in fig. 3a. This observation is partly attributed to the alignment of the hot wires that gives a longer distance for the wake to develop downstream of the troughs than downstream of the peaks. Using a corrected downstream position, x^* defined as $x^* \equiv (x + A(z))$, hence allows comparison of these span-wise positions without the bias of this downstream offset.

Fig. 4 shows the downstream evolution of the maximum velocity deficit, $\overline{U}_0$, and the semi-wake width, Δ, at the three span-wise locations, based on x^*. The semi-wake width is defined as the width of the wake at half of its maximum velocity deficit, following Hah $et\ al.$[20]

Fig. 4a shows that for $0.25 < x^*/c < 1.75$, the velocity deficits are all very similar. However, the wake widths, plotted on fig. 4b, are higher for the trough than for the peak, for the whole range of downstream positions. Although the trend of velocity deficit for the mid-point's wake is hard to distinguish from the trough, the wake width clearly lies between the peak and trough. Since the wake inhomogeneity is persistent far downstream, it is not possible to solely explain the difference with the downstream distance offset, and another explanation must be given.

Fig. 5 shows $y - z$ planes of span-wise velocity and stream-wise vorticity, obtained from the PIV measurements, downstream of $S20W84B$ and $S20W40B$ at $x/c = 0.4$. The main feature is the existence of a
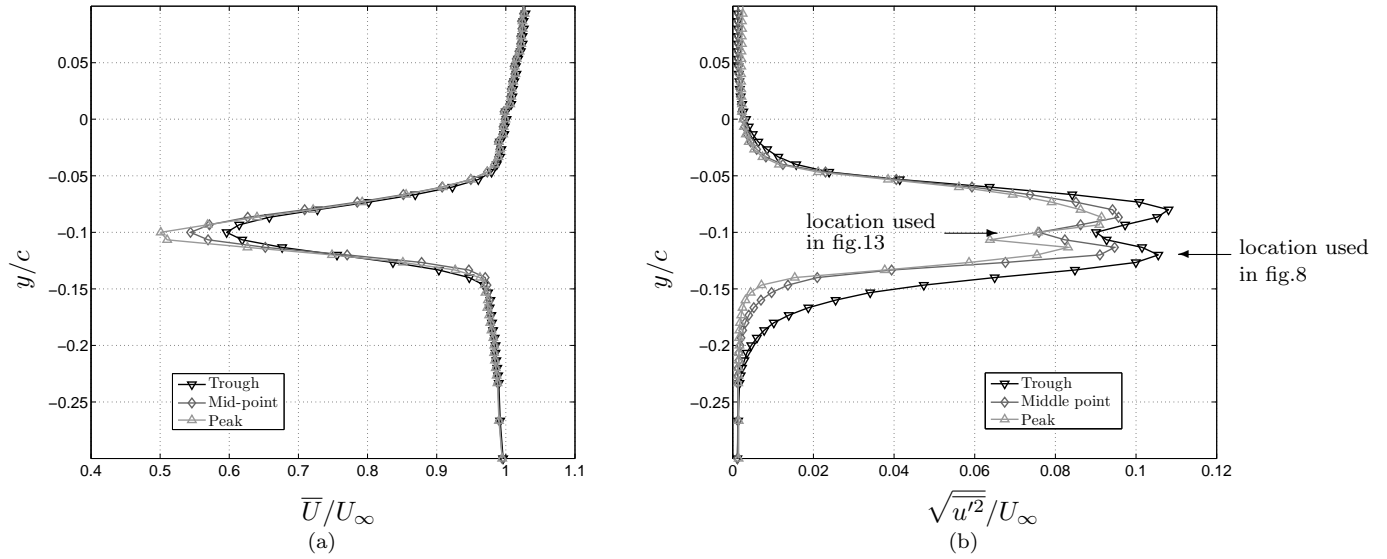
Figure 3: Mean (a) and RMS (b) wake velocity profiles at $x/c = 0.04$ for three span-wise locations behind $S20W84B$.
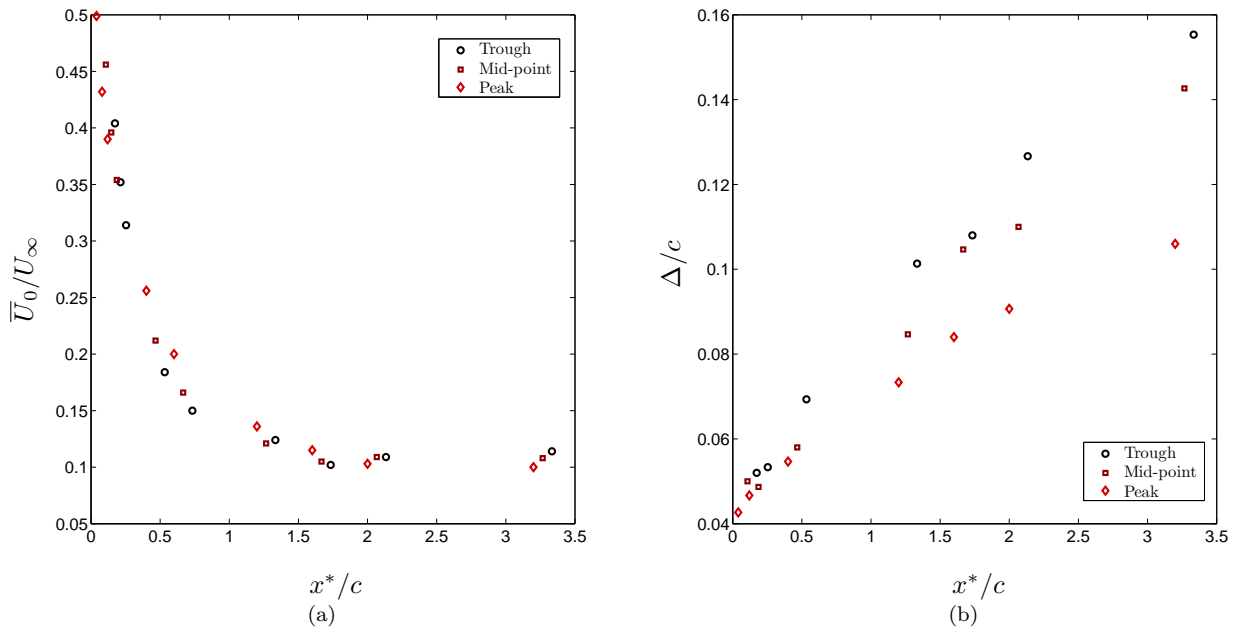

Figure 4: Downstream evolution of maximum velocity deficit (a) and semi-wake width (b) at three span-wise locations for $S20W84B$.

span-wise flow from under the peaks towards the troughs, which induces stream-wise vorticity as illustrated in fig. 5b and 5d. However, the counter flow that one could expect from above the trough toward the peak is much weaker, which indicates that overall the added span-wise component tends to push the flow into the

American Institute of Aeronautics and Astronautics

troughs. Although the span-wise flow covers a high vertical extent for $S20W40B$, both cases display very similar patterns and show a good repeatability between successive peaks for $S20W40B$.

The pressure difference between the pressure and suction sides of the lifting wing explains the creation of this span-wise flow on the sides of the cut-in sinusoids. In turn, this flow would re-energise the wake behind the trough while increasing the velocity deficit behind the peak. This flow structure is consistent with the behaviour observed in fig. 4.
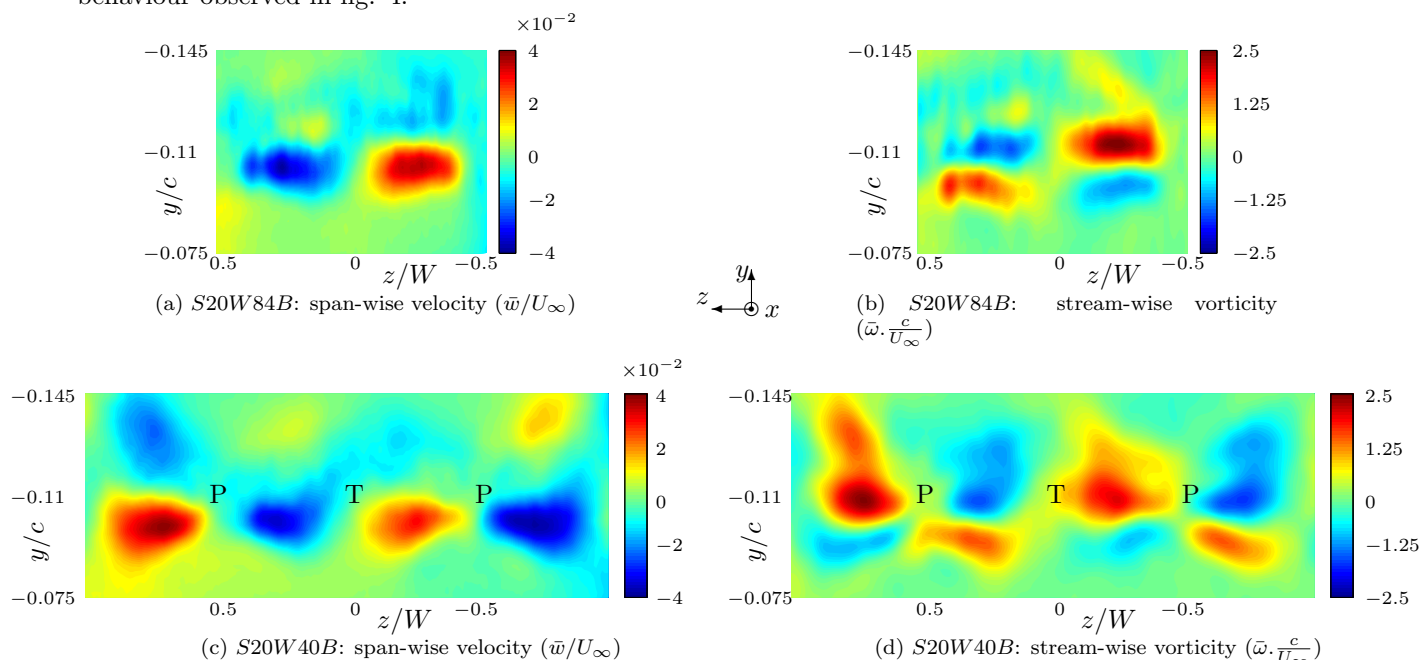

(a) $S20W84B$: span-wise velocity ($\bar{w}/U_\infty$)

(b) $S20W84B$: stream-wise vorticity ($\bar{\omega}.\frac{c}{U_\infty}$)

(c) $S20W40B$: span-wise velocity ($\bar{w}/U_\infty$)

(d) $S20W40B$: stream-wise vorticity ($\bar{\omega}.\frac{c}{U_\infty}$)

Figure 5: PIV maps of mean velocity span-wise component and mean stream-wise vorticity at $x/c = 0.4$. TE peaks (P) and troughs (T) locations indicated on the maps.

In summary, fig. 4 and 5 show that the mean properties exhibit a clear and persistent inhomogeneity of the wake in the span-wise direction, due to a peak-to-trough added flow.

B.   Spectral analysis

Given that we introduce bluntness in the trailing edge, an important question is the identification of unsteady shedding phenomena, and whether the previously discussed span-wise inhomogeneity is also clear in this aspect. Firstly, three TE with the same maximum bluntness are investigated: the straight blunt and two wavelengths of blunt sinusoidal TEs. Fig. 6 displays maps of spectra for vertical traverses at the same downstream position, $x/c = 0.04$ behind the troughs of $S20W00B$ (6a), $S20W84B$ (6c) and $S20W40B$ (6e). Fig. 6b, 6d and 6f correspond to the sharp cases, which will be discussed later in section D. The value plotted is the PSD normalised by $U_\infty.c$, a product of two external parameters which allows direct comparison between different cases. The Strouhal number, St, is based on the maximum bluntness in the

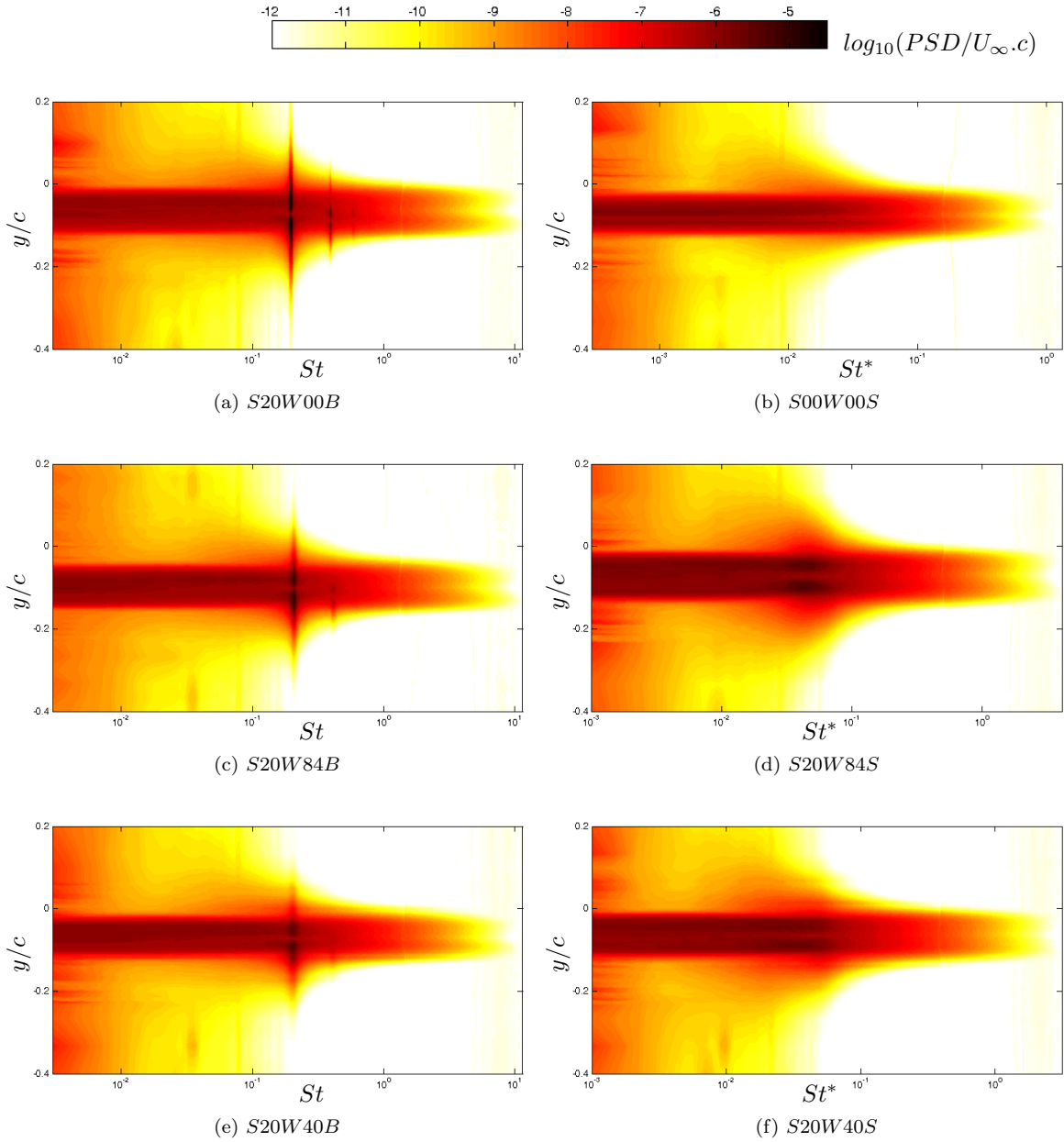trough, $h = 5.5\,\mathrm{mm}$, similar to the study of Tombazis & Bearman.[8]

Figure 6: Vertical PSD log_{10} map at $x/c = 0.04$ behind the 6 studied TE troughs

Fig. 6 shows a clear shedding at $St = 0.18$ for $S20W00B$, which is close to the value obtained by Nedić and Vassilicos.[17] There is a trend of increasing St with decreasing wavelength, to $St = 0.186$ for $S20W40B$ and $St = 0.19$ for $S20W84B$. A similar trend was also reported for triangular serrations.[17] In addition, shedding intensity is also seen to depend on the TE wavelength: the second harmonic is visible on fig. 6a for $S20W00B$ while for $S20W84B$, fig. 6c shows a milder main peak and only the first harmonic is visible. For the shortest wavelength, the main peak is again milder while the first harmonic has almost disappeared from fig. 6e. To quantify this trend, one can define the energy associated with the shedding in the wake -

American Institute of Aeronautics and Astronautics

similarly to Rind & Castro[21] and Nedić et al.[22] - by:

$$E_{shedd} = \int_{\mathbb{Y}} \int_{St_{sh}(1-\Delta St/2)}^{St_{sh}(1+\Delta St/2)} \frac{PSD}{U_\infty.c} \, dSt \, d\frac{y}{c}, \tag{2}$$

with $\mathbb{Y}$ being the extent of the vertical traverse, ΔSt the range of Strouhal number over which to integrate and St_{sh} the vortex shedding value of St. The value $\Delta St = 0.2$ is chosen after a sensitivity analysis, illustrated in fig. 7, and corresponds to the value at which the evolution of E_{shedd} becomes linear with ΔSt.
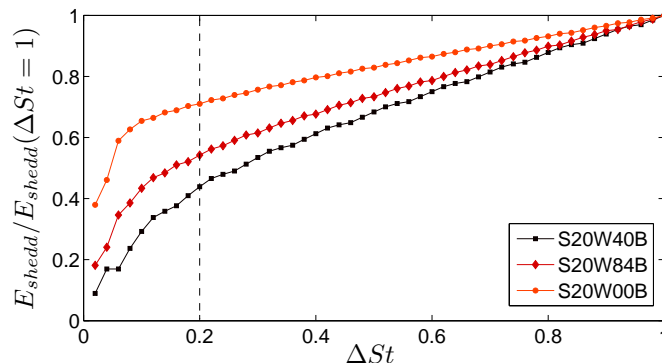

Figure 7: E_{shedd} sensitivity to ΔSt.

With the above definition, the energy associated with shedding shows a reduction of 39% is obtained between $S20W00B$ and $S20W84B$, and 57% between $S20W00B$ and $S20W40B$. It is consistent with a reduction of vortex shedding intensity[17] and associated noise for smaller wavelengths, as reported by Chong et al.,[16] and can be explained by the flow mixing generated by the span-wise flow discussed in section A.

Fig. 6 a, c & e show a slight asymmetry in the wake since the shedding is stronger in the lower half, corresponding to downstream of pressure surface. This is particularly visible for $S20W84B$ and $S20W40B$ and for the harmonics in all cases. This observation is consistent with higher span-wise velocity observed in the lower half of the wake in fig. 5.

The span-wise inhomogeneity of the mean flow seen in fig. 3, 4 and 5 is also expected in the spectra, as the troughs, mid-points and peaks inherently exhibit different physical phenomena. Fig. 8a shows individual spectra measured at $x/c = 0.04$ downstream of $S20W84B$ and $S20W40B$ at three span-wise positions, with a vertical shift for ease of representation. To allow a fair comparison of spectra, at each span-wise location, the vertical position is taken to match the lower peak in the turbulence intensity profiles, such as illustrated in fig. 3b. Although the spectra downstream of the trough in fig. 8a clearly contain energy in a narrow shedding band, the spectra downstream of the peak does not show a clear shedding peak at all. Fig. 8b shows that further downstream, at $x/c = 2$, there is still a difference in the global shape of the spectra between trough and mid-point on one hand and peak on the other hand. This difference is observed even though the shedding spike has disappeared from all three spectra. However, we see that the

difference between spectra downstream of the three span-wise positions is reduced when the wavelength is small. Indeed, the spectra downstream of the trough and the mid-point are almost identical for $S20W40B$ at $x/c = 0.04$. At $x/c = 2$, the smallest wavelength shows a good collapse of spectra for all span-wise positions.

(a) Spectra of $S20W84B$ (top) and $S20W40B$ (bottom) at $x/c = 0.04$

(b) Spectra of $S20W84B$ (top) and $S20W40B$ (bottom) at $x/c = 2$

(c) Downstream evolution of spectra values at St_{sh} for $S20W84B$

(d) Downstream evolution of spectra values at St_{sh} for $S20W84B$, comparison with $S20W40B$ (blue filled symbols) at two downstream positions normalised by W
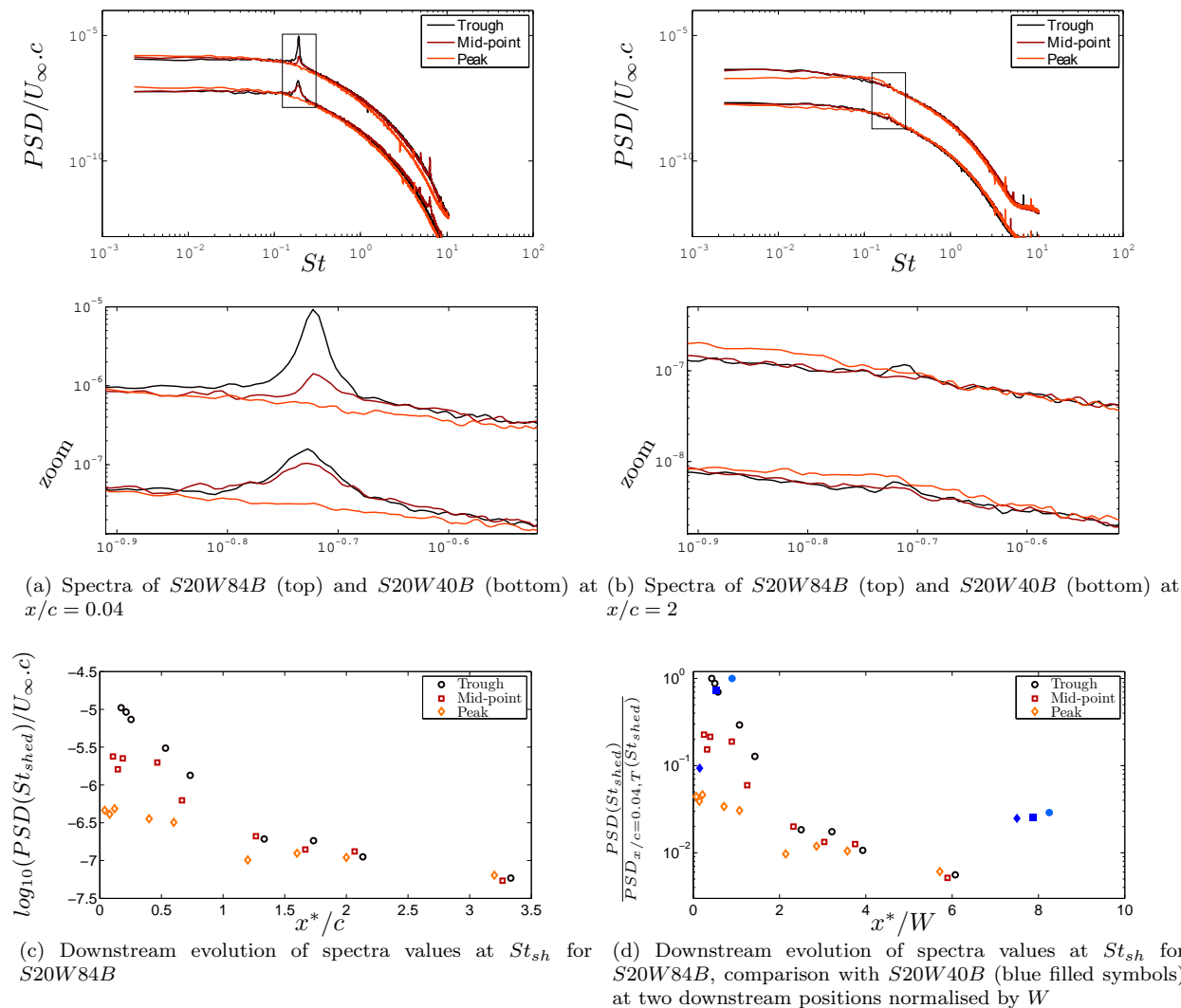
Figure 8: Spectra at three span-wise positions for $S20W84B$ and $S20W40B$ at $x/c = 0.04$ (a) and $x/c = 2$ (b). Inserts show a zoom around St_{sh}. Downstream evolution of spectra values at St_{sh} for $S20W84B$ (c).

To study how this span-wise variation evolves in the wake, fig. 8c shows the downstream evolution of the maximum shedding spike value in the wake of $S20W84B$. The spectra downstream of the peak do not exhibit a shedding spike, hence the values of the spectra at St_{sh} are plotted in this figure. As previously observed, the shedding intensity is higher behind the trough than behind the mid-point close to the trailing edge. This difference vanishes around $x^*/c = 1.5$, after which both shedding intensities stay very similar, and continue to decrease. The farthest downstream points, at $x^*/c > 3$, give a value 2 orders of magnitude lower than the initial value, and indeed the shedding peaks are then barely discernible in the spectra.

One would expect that the TE wavelength will affect the inhomogeneity in the wake, and for this, fig.

American Institute of Aeronautics and Astronautics

8d shows the same evolution as fig. 8c, with the downstream distance normalized by W instead of c. The PSD values at shedding frequency are also plotted for $S20W40B$ at two downstream positions. Despite the value of trough and mid-point being closer for $S20W40B$ at small x^*/W values, a strong difference between mid-point and peak is also observed. Thus, at comparable x^*/W values, the smaller TE wavelength also exhibits span-wise inhomogeneity.

The results presented so far were measured at fixed span-wise locations. Given the strong variations observed, measurements with smaller separations have also been performed. Fig. 9 shows the PSD maps of span-wise traverses behind $S20W40B$, $S20W84B$, $S20W00B$ and $S00W00S$ (discussed in section D) at $x/c = 0.04$. Measurements were done in the middle (cross-stream direction) of the wake, taken as the point of locally minimum turbulence intensity. For $S20W40B$, only half of the traverse is displayed for ease of comparison, however symmetry was checked on the full extent of $-1 < z/W < 0$. The differences of shedding intensity noted for cross-stream traverses in fig. 6 are also visible here, with $S20W40B$ having the mildest intensity. Both straight wings exhibit a span-wisely homogeneous map. For both $S20W40B$ and $S20W84B$ the spectra maps show no shedding signature behind the peak ($z/W = -0.5$) and an increasing intensity towards the troughs. One notices that the trough to peak variation is not monotonic, which is particularly visible in 9a.

Following on the comments made for fig. 8 & 9, one should study the span-wise homogeneity of the shedding signal at various downstream positions. For each downstream position, the shedding energy is obtained as a function of z by integrating the normalised spectra around the shedding value of St, which corresponds to the frequency-integration in Eq.(2). Fig. 10 shows the outcome of these measurements for $S20W84B$ and $S20W40B$. The shedding energy levels decrease when going downstream reaching low values at positions *circa* $x/c = 1.5$, at which according to fig. 8 no shedding spike is discernible. Until reaching the lowest values of $E_{shed}(z)$, the traverses exhibit span-wise variations in both cases.

Therefore, the results presented in both fig. 8 and fig. 10 show that the wakes behind $S20W84B$ and $S20W40B$ do not reach span-wise homogeneity of shedding intensity, even at relatively large downstream distances, where in fact the shedding signal vanishes before this state is reached.

C.   Coherence

The observation of a distinct shedding in the evolving wake of the wings indicates the possible existence of a span-wisely coherent vortex street; which is linked to three topics of interest. Firstly, blunt trailing edges with castellated patterns show a reduction of base drag associated with the conversion of span-wise vorticity into stream-wise vorticity,[6] which would translate into partially breaking down the span-wisely coherent vortex street. Secondly, in the case of wake-blade interaction (i.e. blades array, gas turbine, wind farm etc.),
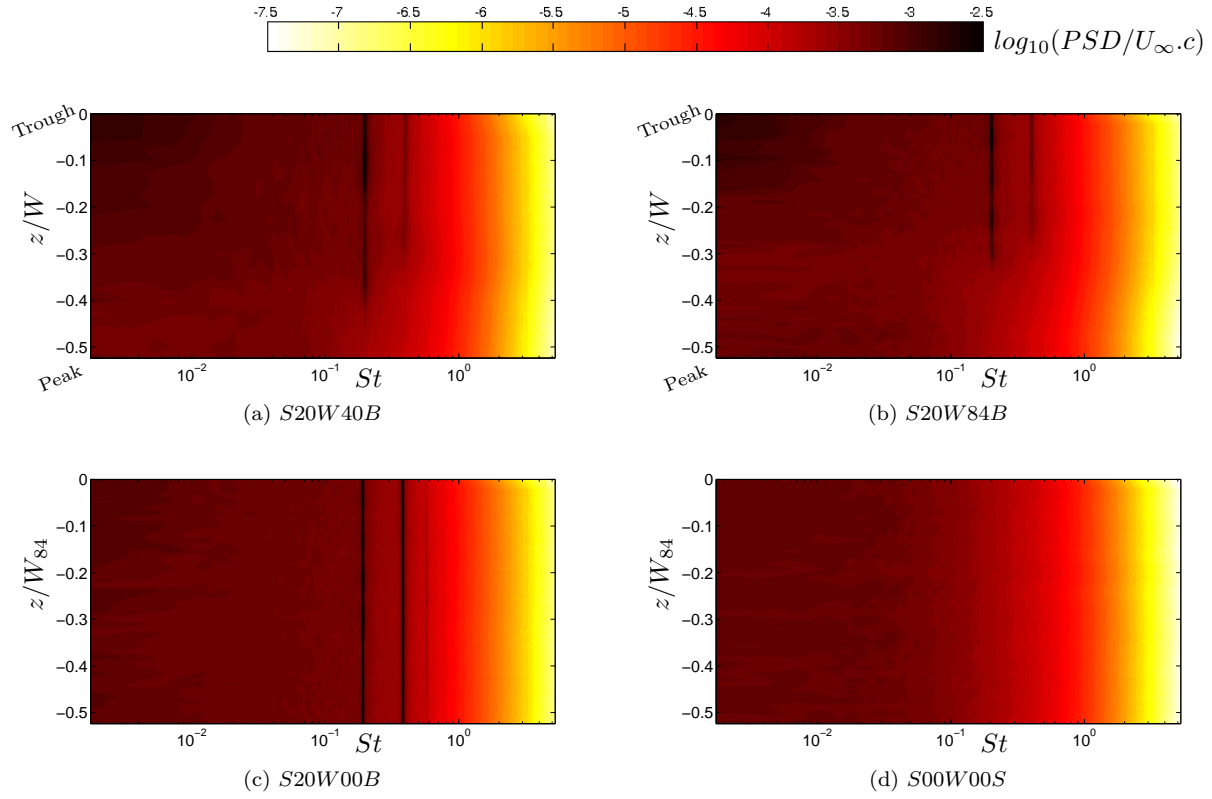
Figure 9: Span-wise PSD log_{10} map at $x/c = 0.04$ behind $S20W40B$, $S20W84B$, $S20W00B$ and $S00W00S$
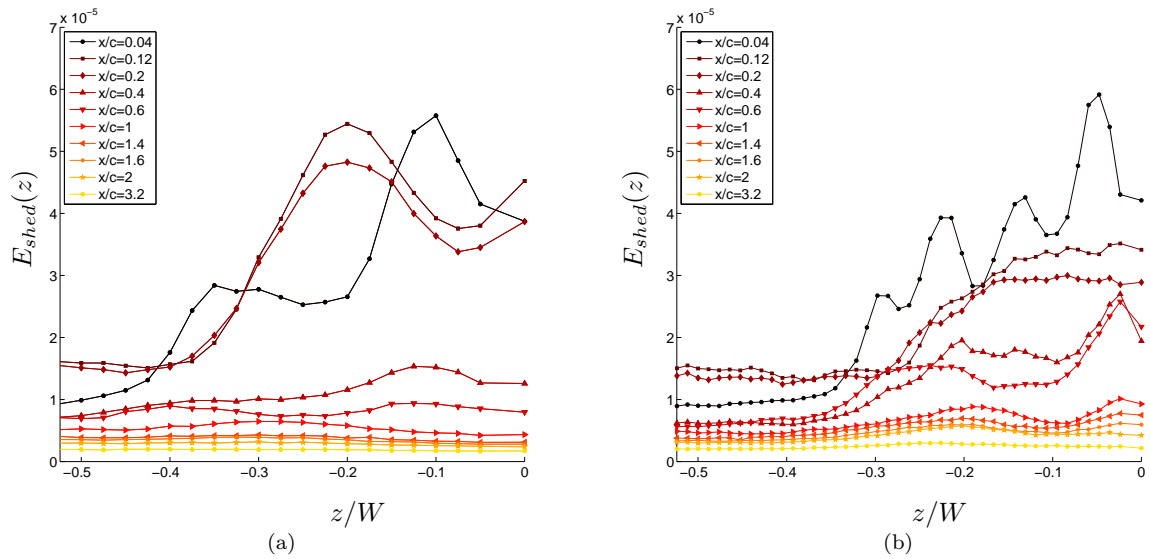

Figure 10: Span-wise traverses of shedding-associated energy. Downstream evolution behind $S20W40B$ (a) and $S20W84B$ (b).

such a vortex street would be detrimental as it would impinge onto the subsequent blade, generating noise and potential structural issues. Finally, span-wise correlation close to the trailing edge can be an indication of acoustic sources.[16]

In order to study the contribution of coherence at different frequencies in the wake, the following definition is taken:

$$\gamma^2 = \frac{|\Phi_{v_1,v_2}|^2}{\Phi_{v_1,v_1} . \Phi_{v_2,v_2}}, \tag{3}$$

where Φ_{v_1,v_2} is the cross-power spectral density between two time series v_1 and v_2.

Fig.11 shows vertical traverses of the two-point coherence between trough and mid-point, and trough and peak, at three downstream positions. Fig. 11a shows that in the wake there is no coherence between trough and mid-point ($W/4$ separation) except around $St = 0.19$ which corresponds to the shedding previously observed. It is also clear that the lower part of the wake exhibits more coherence at this value than the upper part. Going further downstream, figs. 11c & 11e, the coherence in the wake decreases and becomes more symmetrical. Figs. 11b, 11d & 11f on the other hand show the appearance of very slight coherence between trough and peak at $St_{shedding}$ when going downstream. This corresponds to the span-wise spreading of shedding when the wake develops, but the value reached at $x/c = 2$ is much lower between trough and peak than between trough and mid-point. This is in fact in line with the comment made on the spectra, with shedding tending to disappear before it could be uniformly spread over the full TE wavelength, as illustrated in fig.8c.

One notices in fig. 11e that coherence between trough and mid-point appears in the wake over a broad range of low frequencies, up to $St = 0.03$. Although the authors suggest it could be due to rib structures developing in the wake, it can not be asserted at this stage of the investigation.

To focus on the downstream evolution of the shedding-associated correlation, fig. 12a shows the downstream evolution of vertical traverses of γ^2 at $St_{shedding}$ between trough and mid-point. Firstly, the strong asymmetry observed between the upper and lower part of the wake at $x/c = 0.04$ has diminished by $x/c = 0.4$ while the maximum values remain close to $\gamma^2 = 0.9$. In a second phase, the correlation slowly diminishes downstream until positions *circa* $x/c = 2$, which correspond to the point where the shedding intensity stops being discernible from the spectra, as pictured in fig.8c. The maximum values then decrease more significantly while going further downstream.

The effect of wavelength on γ^2 at $St_{shedding}$ is illustrated in fig.12b, with vertical traverse for $S20W84B$, $S20W40B$ and $S20W00B$ (whose probes' positions are based on the former TE). The straight blunt case exhibits high values of γ^2 over a large y-extent, which denotes coherence that is more persistent outside of the wake. Both sinusoidal cases have a shorter y-extent of high γ^2 values, but the maximum is higher than for the straight; 0.85 to 0.9 for $S20W84B$. One should keep in mind, though, that due to the smaller wavelength
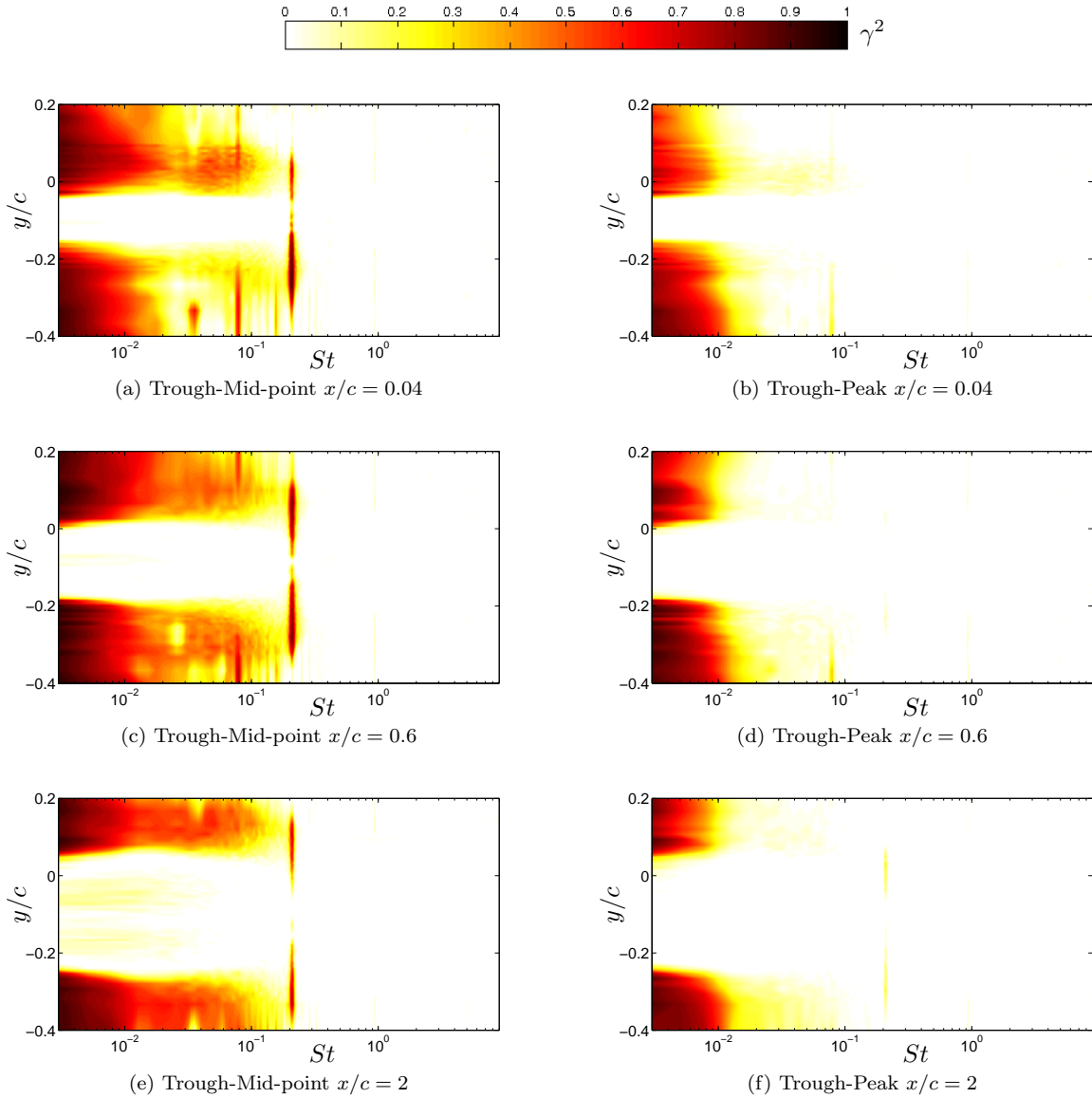
Figure 11: γ^2 map between Trough and Mid-point, and Trough and Peak, behind $S20W84B$ at given downstream locations

of $S20W40B$, the probes are closer than in the case of $S20W84B$ and $S20W00B$ since they match the trough and mid-point positions. This shorter separation ($W/4$) could explain the higher maximum value observed for $S20W40B$. Compared to a straight blunt TE, the sinusoidal cut-in TEs reduce coherence in the wake close to the trailing edge. A marginally higher maximal value is observed in the traverse, but the y-extent over which coherence is measured is reduced for the sinusoidal TEs.

To look at smaller scale correlations, a span-wise traverse is performed with a reference point on the centreline behind a trough and a second point traversed away in the span-wise direction. Fig. 13 shows the map of γ^2 measured at $x/c = 0.04$ and in the middle of the wake (as illustrated in fig. 3b), which is at the height of the trailing edge tip. Fig. 13b shows a band of correlation at the shedding frequency behind $S20W84B$, that spans from the trough to the mid-point and disappears before the peak, which is consistent with fig. 11a & 11b. Compared to a straight blunt TE, both sinusoidal TEs exhibit a reduction of correlation at the shedding frequency. This reduction can be seen even more clearly by comparing respective harmonics.

However, both sinusoidal TEs have a higher correlation in the trough (top left corner of the γ^2 plots in fig. 13) at low frequency compared to $S20W00B$. Given the span-wise extent over which this is noticeable, a logical explanation is the span-wise flow, offspring of the cut-in approach observed in fig. 5. Having a higher mixing in the near wake to reduce shedding thus comes at the price of an increased coherence at low frequency. This flaw is reduced with the shorter wavelength, which has a lower maximal value and a smaller physical extent (W being smaller) of coherence.

Compared to a straight blunt TE, the sinusoidal cut-in TEs thus appear to reduce span-wise coherence in the wake close to the trailing edge, in both vertical and span-wise extents.

D.   Sharp trailing edge geometry approach

The cut-in approach followed to obtain the sinusoidal trailing edge inherently produces bluntness at the troughs which causes vortex shedding and coherence at the corresponding St_{shedd}. In order to keep the structural benefits of this approach and to mitigate the undesirable effects, a new design is introduced for the trailing edges. Instead of directly cutting into the wing, its aft part is modulated with a sinusoidal pattern, leaving the airfoil section unmodified at the peaks and introducing a steep trailing edge at the trough. Table 1 provides an illustration of this approach. This modification introduces some inherent waviness to the surface of the trailing edge, which may have some impact on account of the important role of span-wise flow in breaking down coherence, as discussed previously. Indeed, wings with rippled trailing edges were studied by Werle and Patterson,[12] who highlighted the presence of span-wise flow on the aft part of such wings.

In order to study the effect of the sharpness on the spectra, vertical PSD traverses have been plotted for
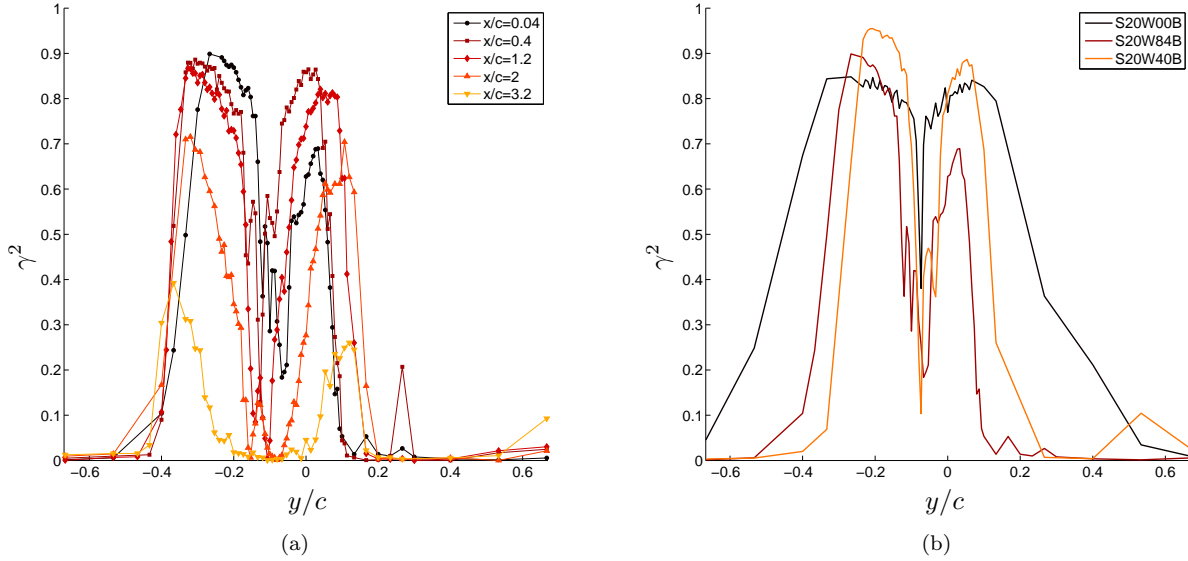
American Institute of Aeronautics and Astronautics

Figure 12: Vertical traverses of $\gamma^2(St_{shedd})$ between two span-wise locations: trough and mid-point. Downstream evolution behind $S20W84B$ (a) and comparison between blunt cases at $x/c = 0.04$ (b).

the sharp TE geometries, alongside the blunt TE in fig. 6. The previous definition of St is not applicable, as h does not represent a real parameter of the sharp cases. instead, one could consider using an 'effective viscous' bluntness, defined as the sum of boundary layer displacement thickness on upper and lower surfaces: $(\delta^*_{pressure} + \delta^*_{suction})$ where the displacement thickness δ^* defined as

$$\delta^* \equiv \int_0^\delta 1 - \frac{\bar{U}}{U_\infty} \, d\frac{y}{c}, \tag{4}$$

since it describes the effective separation between the two meeting shear layers. Given that the free stream has a velocity gradient, the usual definition of δ could not be used. The kurtosis of u' has two plateaux, in both the boundary layer and the free stream; the limit between them being marked by a spike in its value. Therefore, the value of δ was determined by using the point of maximum kurtosis of velocity fluctuation when traversing away from the boundary layer. When focusing on the blunt cases, it is observed that the use of both $\delta^*_{pressure}$ and $\delta^*_{suction}$ gives scattered values of Strouhal number, which are collapsed if only $\delta^*_{pressure}$ is used. Therefore, $St^* = f.\delta^*_{pressure}/U_\infty$ is used for the sharp case. Hot-wire measurements were conducted in the boundary layer in order to obtain these values.

Fig. 6d and 6f show the PSD map for $S20W84S$ and $S20W40S$ respectively, at $x/c = 0.04$. The spectrum map displays a region of higher intensity, more broadband than in the blunt cases (Fig.6 a,c,e) and no harmonic is seen. The maximum values are also lower than in the blunt case.

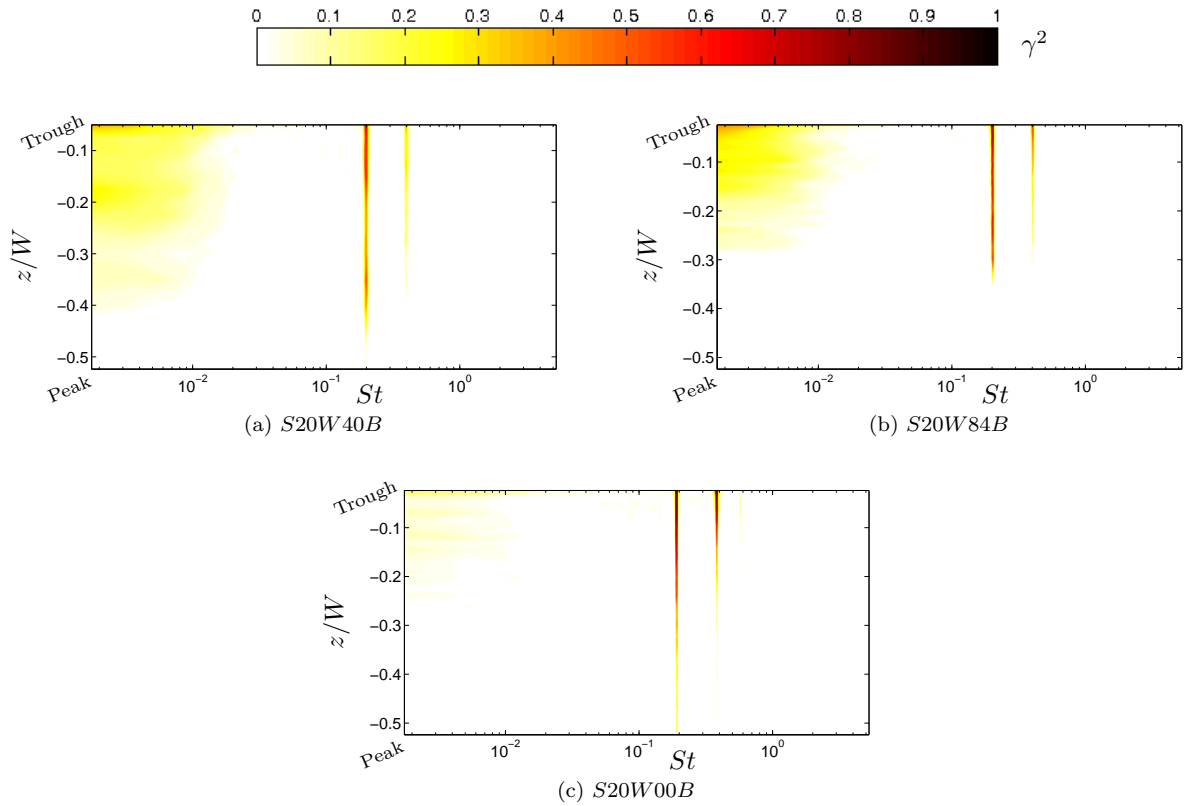Fig. 14 compares the spectra between blunt and sharp trailing edges for both wavelengths at a given

American Institute of Aeronautics and Astronautics

Figure 13: Span-wise γ^2 map at $x/c = 0.04$ behind $S20W40B$, $S20W84B$ and $S20W00B$. The reference probe is fixed at the trough ($z/W = 0$) while the second probe is traversed towards the peak ($z/W = -0.5$).

vertical position. The spectra are plotted against frequency, as St^* was observed not to collapse the spectra. The sharp spectra have indeed lower maximum values and more broadband bumps than the blunt, and a shift towards lower frequencies is observed. This observation is consistent with Zobeiri *et al.*,[23] who studied the vortex shedding from an oblique trailing edge on a hydrofoil and observed a lower shedding frequency than with a blunt trailing edge. The design of the sharp TE in our study could be locally seen as an oblique shape, which would explain the shift we observe. As for the more broad-band nature of the bump in the spectra, a possible explanation is that the waviness of the surface locally increases mixing and therefore alters the single tone characteristic.

Fig. 15 shows vertical traverses of coherence between trough and mid-point at a position $x/c = 0.04$ downstream $S20W84S$, $S20W84B$ and $S00W00S$ (the probes' positions being based on the former TE). Contrary to the blunt case, $S20W84S$ does not display coherence in the wake area, over $W/4$ extent, even around the value of St^* for the bump seen in the spectra. In this sense, the coherence between trough and mid-point behind $S20W84S$ is very similar to that of the unmodified wing, if not for a slightly wider y-extent with no correlation at all. When comparing figs 15b and 15c, one sees that a reduction of correlation is achieved over a broad range of St on the edges of the wake between $S00W00S$ and $S20W84B$, at the cost of

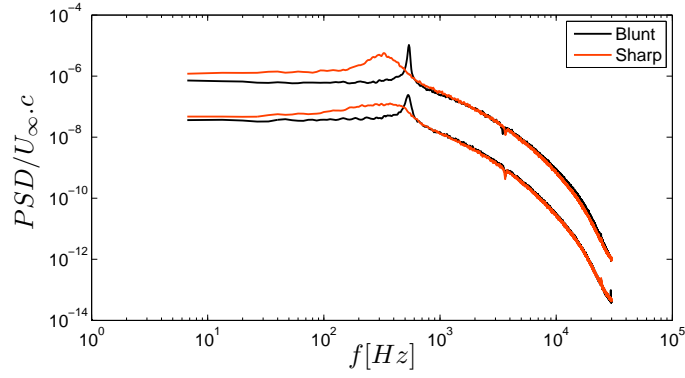American Institute of Aeronautics and Astronautics

Figure 14: Spectra of $S20W84B$ & $S20W84S$ (top) and $S20W40B$ & $S20W40S$ (bottom), at $x/c = 0.04$

a high correlation at the shedding Strouhal number. $S20W84S$ does not achieve such a significant broadband reduction, but the absence of correlation at a discrete shedding frequency in the wake is encouraging for further studies.
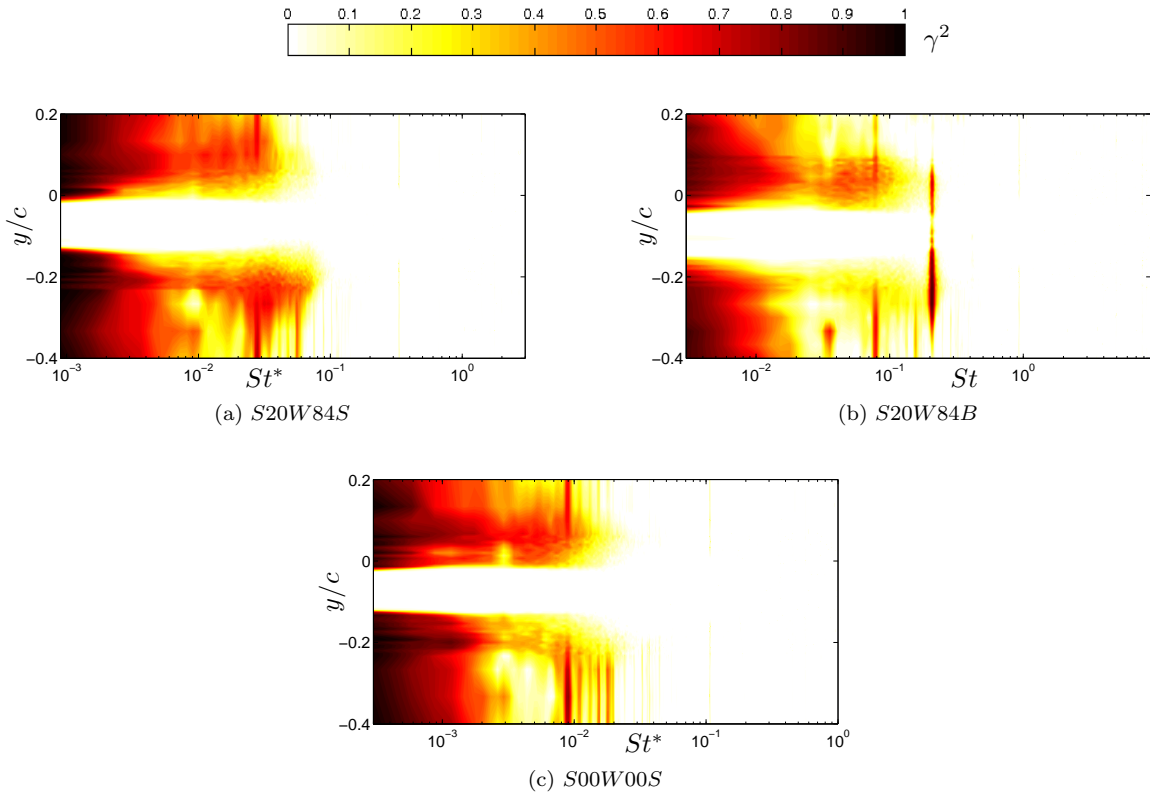

(a) $S20W84S$

(b) $S20W84B$

(c) $S00W00S$

Figure 15: γ^2 map (Trough - Mid-point) behind $S20W84S$, $S20W84B$ and $S00W00S$ at $x/c = 0.04$

IV.   Conclusions

Experiments have been conducted on a NACA0012 wing at moderate angle of attack to study the impact of cut-in sinusoidal trailing edge modifications on the wake generated by a lifting body.

American Institute of Aeronautics and Astronautics

The cut-in approach for the trailing edges generates a flow from below the peaks towards the troughs. Such a flow pattern increases the velocity deficit behind the peaks while re-energising the wake behind the troughs. Therefore, span-wise inhomogeneity of velocity deficit and wake width is observed and persists far downstream, particularly for the wake width.

Span-wise inhomogeneity is also observed in spectral analysis, where the shedding signature slowly spreads out, in the span-wise direction from the troughs. Downstream evolution of the shedding intensity shows that the shedding signature disappears from the spectra before span-wise homogeneity is reached. Furthermore, the shedding intensity strongly decreases with shorter wavelength of the sinusoidal patterns, with up to 57% reduction compared to the straight blunt case.

The span-wise correlation is in turn affected by the modified TE, with a significant reduction of correlation compared to the straight blunt case, and moderate reduction on the wake's edges compared to the unmodified wing. In the wake of the blunt wings, span-wise correlation is mostly seen at the shedding St and is greatly reduced by the sinusoidal patterns compared to the blunt straight one, which opens the door to possible reduction with more complex multiscale geometries.

Tests with a sharp sinusoidal trailing edge were also performed as a first step towards mitigating some of the adverse effects encountered with the cut-in design. The wavy surface and sharpness at the trough of this new design were observed to create a more broadband shedding signature at a lower frequency than the blunt case. Unlike the blunt TE, this design does not exhibit a coherence band in its wake over a length scale of a quarter of a wavelength.

The use of a sinusoidal cut-in trailing edge thus offers promising improvements in terms of reducing the vortex shedding intensity and the span-wise correlation compared to a straight blunt trailing edge. In comparison to an unmodified wing, possible benefits on broadband coherence are mitigated by strongly increased coherence at a discrete shedding frequency, corresponding to $St \approx 0.19$. The span-wise inhomogeneity of wake width and velocity deficit shows the possible use of these patterns in tailoring the wake structure for wake-blade interactions.

Future studies of interest include an assessment of the aerodynamic performance of such modified wings and the use of more complex trailing edge geometries to further reduce undesirable correlation.

Acknowledgments

American Institute of Aeronautics and Astronautics

References

[1]Smith, H. A. and Schaefer, R. F., "Aerodynamic characteristics at Reynolds numbers of 3.0×10^6 and 6.0×10^6 of three airfoil sections formed by cutting off various amounts from the rear portion of the NACA 0012 airfoil section", *NACA TN-2074*, 1950.

[2]Hoerner, S.F. and Borst, H.V., "Fluid-dynamic lift: practical information on aerodynamic and hydrodynamic lift", *NASA STI/Recon Technical Report A*, Vol. 76, 1975, pp. 32167.

[3]Sato, J. and Sunada, Y., "Experimental research on blunt trailing-edge airfoil sections at low Reynolds numbers", *AIAA Journal*, Vol. 33, No. 11, 1995, pp. 2001-2005.

[4]Standish, K. J. and van Dam, C. P., "Aerodynamic Analysis of Blunt Trailing Edge Airfoils", *Journal of Solar Energy Engineering*, Vol. 125, No. 4, 2003, pp. 479-487.

[5]Tanner, M., "A method for reducing the base drag of wings with blunt trailing edge", *DTIC Document No. DFVLR-Sonderdruck-219*, 1970.

[6]Petrusma, M. and Gai, S. L., "Investigation into the wakes of blunt trailing edge aerofoils at low reynolds numbers", *Proceedings of the 10th Australasian fluid mechanics conference*, University of Melbourne, 1989, pp. 35-38.

[7]Krentel, D. and Nitsche, W., "Investigation of the near and far wake of a bluff airfoil model with trailing edge modifications using time-resolved particle image velocimetry", *Experiments in Fluids*, Vol. 54, No. 7, 2013, pp. 1-16.

[8]Tombazis, N. and Bearman, P. W., "A study of three-dimensional aspects of vortex shedding from a bluff body with a mild geometric disturbance", *Journal of Fluid Mechanics*, Vol. 3301997, pp. 85-112.

[9]Johari, H., Henoch, C. W., Custodio, D. and Levshin, A., "Effects of Leading-Edge Protuberances on Airfoil Performance", *AIAA Journal*, Vol. 45, No. 11, 2007, pp. 2634-2642.

[10]Miklosovic, D. S. and Murray, M. M. and Howle, L. E. and Fish, F. E., "Leading-edge tubercles delay stall on humpback whale (Megaptera novaeangliae) flippers", *Physics of Fluids*, Vol. 16, No. 5, 2004, pp. L39-L42.

[11]Fish, F. E. and Lauder, G. V., "Passive and active flow control by swimming fishes and mammals", *Annual Review of Fluid Mechanics*, Vol. 38, 2006, pp. 193-224.

[12]Werle, M. J. and Paterson, R. W., "Trailing-Edge Separation/Stall Alleviation", *AIAA Journal*, Vol. 25, No. 4, 1986, pp. 624-626.

[13]Howe, M.S., "Aerodynamic noise of a serrated trailing edge", *Journal of Fluids and Structures*, Vol. 5, No. 1, 1991, pp. 33-45.

[14]Sandberg, R. D. and Sandham, N. D., "Direct numerical simulation of turbulent flow past a trailing edge and the associated noise generation", *Journal of Fluid Mechanics*, Vol. 596, 2008, pp. 353-385.

[15]Oerlemans, S. and Fisher, M. and Maeder, T. and Kögler, K., "Reduction of Wind Turbine Noise Using Optimized Airfoils and Trailing-Edge Serrations", *AIAA Journal*, Vol. 47, No. 6, 2009, p. 1470-1481.

[16]Chong, T. P., Vathylakis, Al., Joseph, P. F. and Gruber, M., "Self-Noise Produced by an Airfoil with Nonflat Plate Trailing-Edge Serrations", *AIAA Journal*, Vol. 51, No. 11, 2013, pp. 2665-2677.

[17]Nedić, J. and Vassilicos, J. C. , "Vortex shedding and aerodynamic performance of an airfoil with multi-scale trailing edge modifications", *AIAA Journal*, in press.

[18]Traub, L. W. and Cooper, E., "Experimental Investigation of Pressure Measurement and Airfoil Characteristics at Low Reynolds Numbers", *Journal of Aircraft*, Vol. 45, No. 4, 2008, pp. 1322-1333.

[19]Brandt, J. B. and Selig, M. S., "Propeller Performance Data at Low Reynolds Numbers", *49th AIAA Aerospace Sciences Meeting*, 2011, pp. 2011-1255.

[20]Hah, C. and Lakshminarayana, B., "Measurement and prediction of mean velocity and turbulence structure in the near wake of an airfoil", *Journal of Fluid Mechanics*, Vol. 115, 1982, pp. 251-282.

[21]Rind, E. and Castro, I.P., "On the effects of free-stream turbulence on axisymmetric disc wakes",*Experiments in Fluids*, Vol. 53, No. 2, 2012, pp. 301-318.

[22]Nedić, J., Supponen, O., Ganapathisubramani, B. and Vassilicos, J. C., "Geometrical influence on vortex shedding in turbulent axisymmetric wakes", *Physics of Fluids*, Vol. 27, No. 3, 2015, pp. 035103.

[23]Zobeiri, A., Ausoni, P. and Avellan, F., "Vortex shedding from blunt and oblique trailing edge hydrofoils", *3rd IAHR International Meeting of the Workgroup on Cavitation and Dynamic Problems in Hydraulic Machinery and Systems*, 2009, pp. 2005-2009.

American Institute of Aeronautics and Astronautics